Expanded View Figures

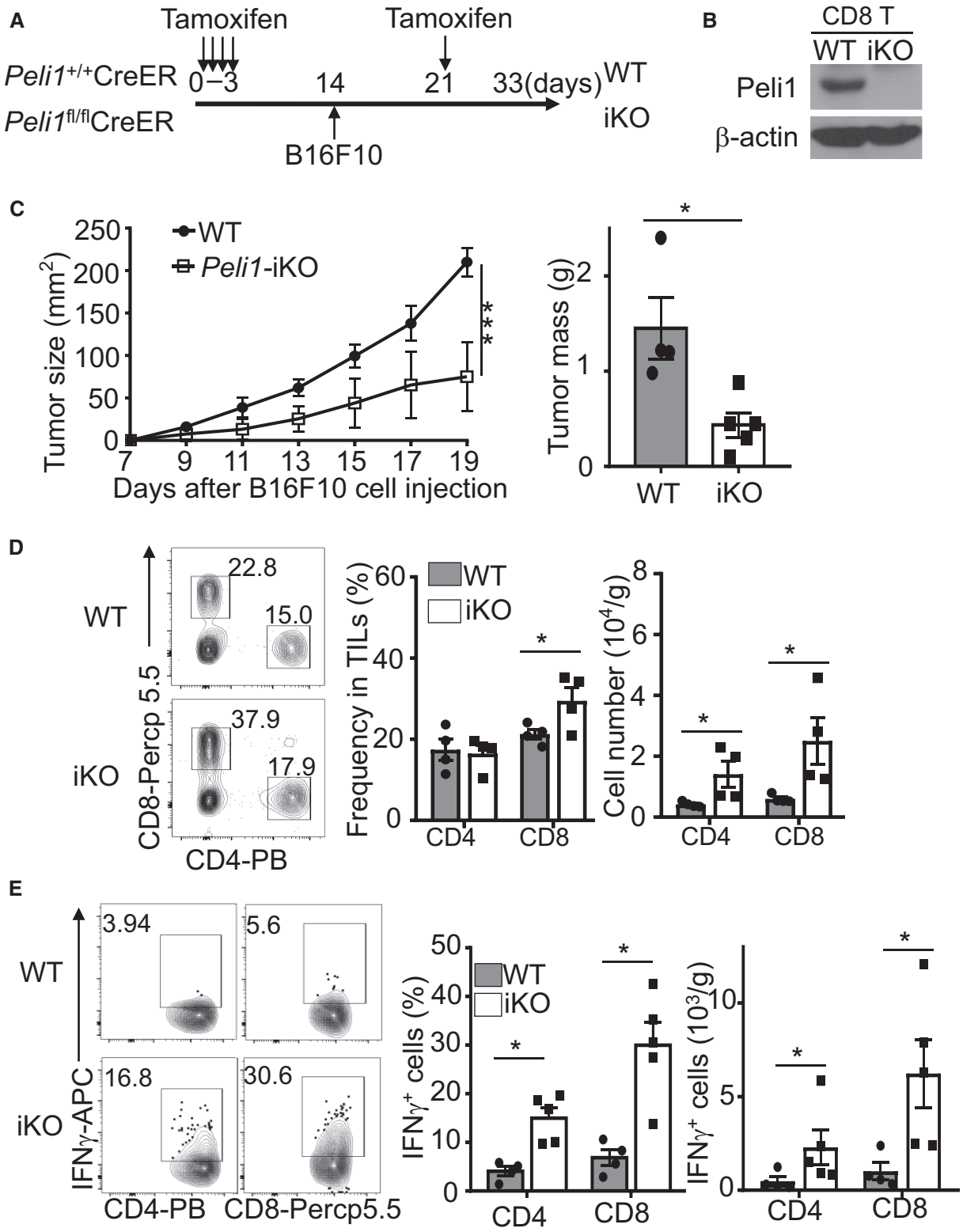

Figure EV1.

Figure EV1. Inducible deletion of Peli1 in adult mice promotes antitumor immunity.

A, B Schematic of experimental design for generating B16F10-bearing Peli1-iKO (iKO) and wild-type (WT) control mice (A) and immunoblot analysis of Peli1 in CD8 T cells of Peli1-iKO and wild-type mice (B).

C Tumor growth curve (left) and summary graph of end-point tumor masses (right) of wild-type ($n = 4$) and Peli1-iKO ($n = 5$) mice inoculated s.c. with B16F10 melanoma cells.

D, E Flow cytometry analysis of total (D, WT: $n = 4$; iKO: $n = 4$) or IFNγ-producing (E, WT: $n = 4$; iKO: $n = 5$) $CD4^+$ and $CD8^+$ T cells in TILs of B16F10 tumor-bearing (day 19) wild-type and iKO mice, presented as a representative plot (left) and summary graph (right).

Data information:: Data are representative of 3 independent experiments, and summary data are presented as mean ± SEM with *P* values being determined by a two-way ANOVA analysis with Bonferroni correction (left panel of C) and two-tailed unpaired Student's *t*-test (right panel of C; D, E). $*P < 0.05$; $***P < 0.001$.

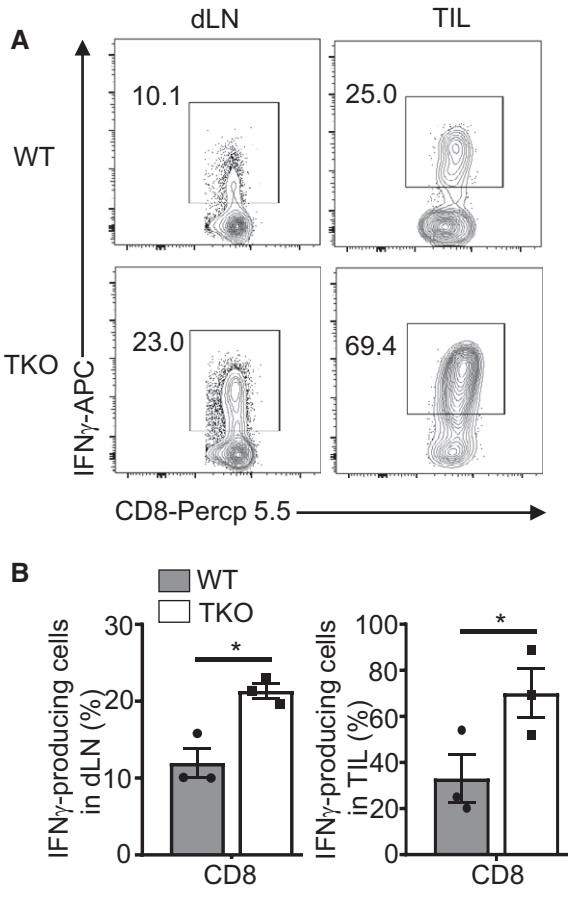

Figure EV2. T cell-specific Peli1 deficiency promotes antitumor immunity in E.G7 tumor model.

A, B Flow cytometry analysis of the frequency of IFNγ-producing CD8 effector T cells in tumor-infiltrating lymphocytes of E.G7 tumor-bearing (day 24) wild-type (WT; $n = 3$) and *Peli1*-KO (TKO; $n = 3$) mice, presented as a representative plot (A) and summary graph (B). Data are representative of 3 independent experiments, and summary data are presented as mean ± SEM with *P* values being determined by two-tailed unpaired Student's *t*-test. $*P < 0.05$.

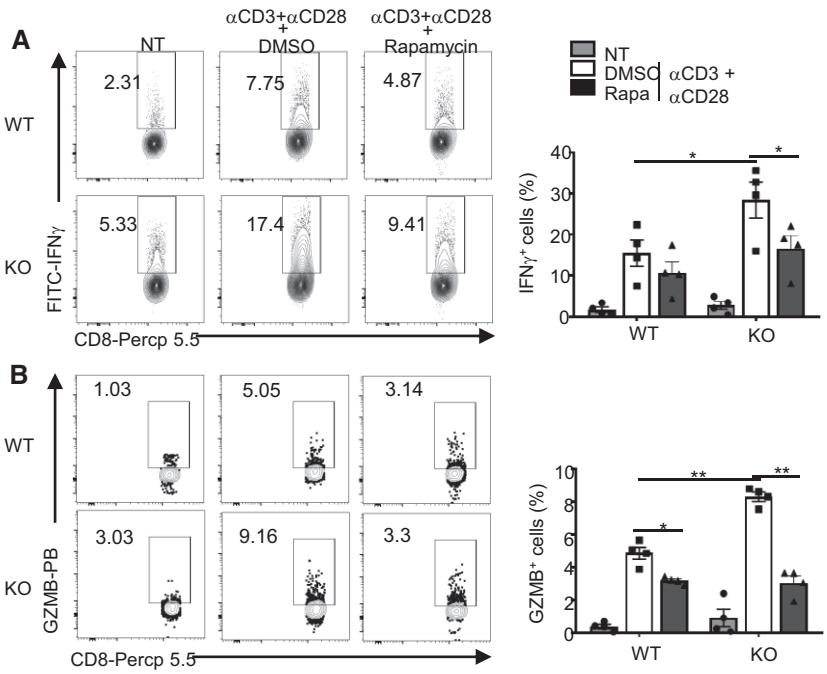

Figure EV3. Hyper-induction of IFNγ and granzyme B in Peli1-deficient CD8 T cells is dependent on mTORC1.

A, B Flow cytometry analysis of intracellular IFNγ (A) and granzyme B (B) in OT-I naïve T cells that were either not treated (NT) or stimulated for 16 h with plate-coated anti-CD3 (1 μg/ml) and anti-CD28 (1 μg/ml) in the presence of DMSO or rapamycin (10 nM). Data are repeated with 4 independent experiments, and the results were presented as a representative plot (left) and summary graph of mean ± SEM values based on multiple mice (right). *P* values were determined by two-tailed unpaired Student's *t*-test. $*P < 0.05$; $**P < 0.01$.

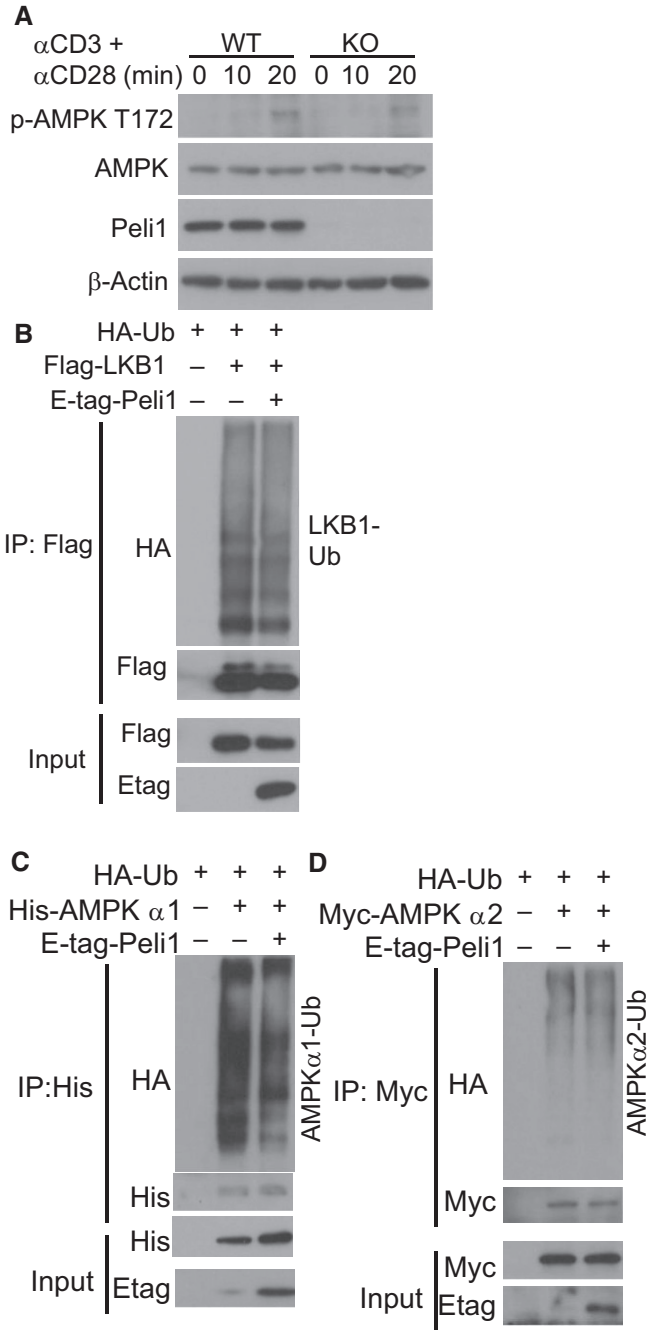

Figure EV4. Peli1 does not regulate AMPK activation or mediate ubiquitination of LKB1 and AMPK.

A Immunoblot analysis of the phosphorylated (P-) and total proteins in whole-cell lysates of CD8 T cells stimulated for the indicated time points.

B–D Ubiquitination of LKB1 (B), AMPKα1 (C), and AMPKα2 (D) in 293 cells transfected with the indicated expression vectors. Ubiquitinated proteins were isolated by immunoprecipitation and detected by immunoblot (upper), and the protein expression levels in input cell lysates was analyzed by immunoblot (lower).

A

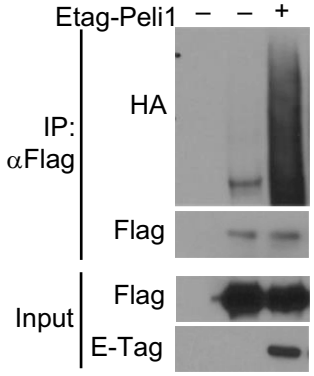

B

Identified residue	Peptide sequence	Residues
Lysine 30	RDDVTAVFK#ENLNSDRG	22-38
Lysine 632	KAK#GNTEEDGVPSTSPMEVLDRL	630-652

C

Species	TSC1 sequence alignment
Human	22 RDDVTAVFKENLNSDRG 38
Mouse	22 RDDVTAIFKESLNSERG 38
Rat	22 RDDVTTIFKESLNSERG 38
Chimpanzee	22 RDDVTAVFKENLNSDRG 38
Dog	22 RDDVTAVFKENLSSDRG 38
Human	630 KAKGNTEEDGVPSTSPMEVLDRL 652
Mouse	627 KVKGNPEEDCVPSTSPMEVLDRL 649
Rat	630 KAKGNPEEDCVPSTSPMEVLDRL 652
Chimpanzee	630 KAKGNTEEDGVPSTSPMEVLDRL 652
Dog	630 KAKGNTEEDYPPSTSPAEVLDRL 652

Figure EV5. Sites of Peli1-mediated TSC1 ubiquitination.

A Immunoprecipitation and immunoblot analysis of TSC1 ubiquitination in 293 cells transfected with (+) or without (–) the indicated expression vectors.

B Summary of ubiquitination sites of TSC1 detected by mass spectrometry in cells coexpressing TSC1 and Peli1. TSC1 was isolated by anti-Flag immunoprecipitation from 293T cells transiently transfected as indicated in (A). Samples from lanes 2 and 3 were analyzed by mass spectrometry.

C Sequence alignment of TSC1 ubiquitination sites.